Backward Phase-Matched Second-Harmonic Generation from Stacked Metasurfaces

Timo Stolt,[1,*] Jeonghyun Kim,[2,*] Sébastien Héron,[3] Anna Vesala,[1] Younghwan Yang,[2] Jungho Mun,[5] Minkyung Kim,[2] Mikko. J. Huttunen,[1] Robert Czaplicki,[4] Martti Kauranen,[1] Junsuk Rho,[2,5,6,‡] and Patrice Genevet[3,†]

[1]*Photonics Laboratory, Physics Unit, Tampere University, FI-33014 Tampere, Finland*
[2]*Department of Mechanical Engineering, Pohang University of Science and Technology (POSTECH), Pohang 37673, Republic of Korea*
[3]*Université Côte d'Azur, CNRS, CRHEA, rue Bernard Gregory, Sophia Antipolis, 06560 Valbonne, France*
[4]*Institute of Physics, Faculty of Physics, Astronomy, and Informatics, Nicolaus Copernicus University, Grudziądzka 5/7, 87-100 Toruń, Poland*
[5]*Department of Chemical Engineering, Pohang University of Science and Technology (POSTECH), Pohang 37673, Republic of Korea*
[6]*National Institute of Nanomaterials Technology (NINT), Pohang 37673, Republic of Korea*

(Received 16 June 2020; accepted 16 December 2020; published 22 January 2021)

We demonstrate phase-matched second-harmonic generation (SHG) from three-dimensional metamaterials consisting of stacked metasurfaces. To achieve phase matching, we utilize a novel mechanism based on phase engineering of the metasurfaces at the interacting wavelengths, facilitating phase-matched SHG in the unconventional backward direction. Stacking up to five metasurfaces,we obtain a phase-matched SHG signal, which scales superlinearly with the number of layers. Our results motivate further investigations to achieve higher conversion efficiencies also with more complex wave fronts.

DOI: 10.1103/PhysRevLett.126.033901

Optical metamaterials and metasurfaces are artificial structures consisting of subwavelength building blocks, known as meta-atoms, and are associated with optical properties not found in nature [1]. These properties include magnetism at optical frequencies, strong optical activity, negative index of refraction, and epsilon-near-zero behavior [2–4]. In addition, recent work on phase-engineered metasurfaces has demonstrated the interesting possibilities to realize flat optical components, such as lenses, holographic components, and polarizers [5–11].

In addition to the linear optical properties of metamaterials, their nonlinear optical responses are also becoming important. Several technologically relevant photonic applications rely on the nonlinear responses of materials, including second-harmonic generation (SHG), photon-pair generation, all-optical switching, frequency combs, and supercontinuum generation [12–15]. The challenging part in these nonlinear applications is the fact that nonlinear optical processes in materials are intrinsically weak. Because of this fact, nonlinear processes in conventional materials, such as crystals, rely on the concept of phase matching. In phase-matched materials and without losses, the generated nonlinear signal scales quadratically on the propagation length, resulting in practical conversion efficiencies with sufficiently long materials [see Fig. 1(a)] [16,17].

For homogeneous materials and forward SHG signals, phase matching can be achieved if the refractive indices at the fundamental and second-harmonic frequencies are equal. However, this requirement is a significant limitation because of refractive-index dispersion, which can be overcome by the concept of quasi-phase-matching, i.e., by structuring the material in such a way that the sign of the nonlinear susceptibility is periodically reversed [18]. In principle, quasi-phase-matching is a very general concept that allows any nonlinear signal to be optimized. Unfortunately, quasi-phase-matching and other traditional phase-matching schemes seem unfeasible for miniaturization of optical devices. Additionally, these techniques are restricted in terms of, e.g., polarization and the spatial

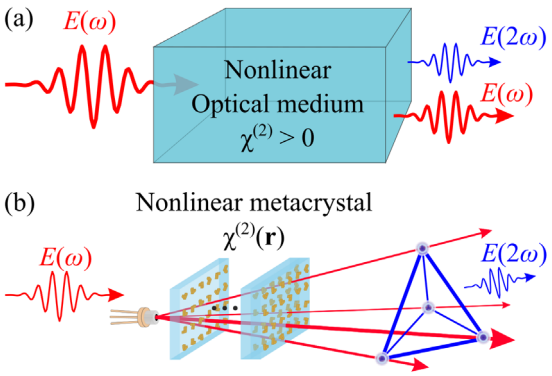

FIG. 1. (a) For traditional nonlinear materials, achieving phase matching and strong nonlinear responses is very restricted in terms of, e.g., the selected material and the polarization of the interacting fields. (b) Nonlinear optical processes can be phase matched with metamaterials that induce arbitrary phase changes in the interacting fields.

profiles of the interacting waves. These limitations motivate the ongoing development of efficient and less restricted nanoscale devices.

Utilization of metal nanoantennas has recently emerged as a promising route toward more efficient nonlinear metamaterials [19,20]. Metal nanoantennas support collective oscillations of conduction electrons, known as localized surface plasmons. Under resonant conditions, these oscillations give rise to localized surface plasmon resonances (LSPRs), which can considerably enhance the local field near the particles [21]. Because nonlinear processes scale with high powers of the local field, the plasmon-assisted field enhancement can result in a dramatic increase in the otherwise weak nonlinear response. Consequently, numerous investigations have been carried out during the past decade in order to understand the nonlinear response of plasmonic nanoantennas [22–26]. So far, work on nonlinear metamaterials has focused on single planar metasurfaces limiting the achieved efficiencies. A viable route to improve the efficiencies, which was explored numerically before [27], would be to stack several metasurfaces on top of each other, giving rise to phase-matching issues. In addition, such nonlinear metamaterials could provide novel capabilities to conventional phase-matching techniques relying on the intrinsic material dispersion. Particularly, the use of metamaterials could allow one to design phase-matched devices exhibiting arbitrary transverse phase profiles, therefore providing interesting possibilities to fabricate nonlinear metalenses and holography [see Fig. 1(b)] [28,29].

We demonstrate how such nonlinear phase-matched metamaterials can be fabricated by stacking metasurfaces into three-dimensional (3D) structures and show how the approach can considerably improve the performance of existing nonlinear metasurfaces. Our approach utilizes both local-field enhancement and phase engineering of LSPRs. The latter provides more freedom to phase match nonlinear processes than what is possible using conventional nonlinear materials [see Fig. 1(b)]. We demonstrate both capabilities by fabricating metamaterial devices consisting of up to five layers of metasurfaces that are phase matched to emit SHG in the backward direction. We demonstrate *superlinear* dependence of the emitted SHG signals on the number of stacked metasurfaces, which is only possible via phase matching.

For conventional materials and SHG, the phase changes are associated with the propagation of the fundamental and second-harmonic fields through the material. Phase matching in such materials is connected to wave vector mismatch Δk, which vanishes for perfectly phase-matched processes. With Δk, we can define the phase-matching condition, e.g., for backpropagating SHG as $\Delta k = 2k_\omega + k_{2\omega} = 0$, where $k_\omega = n_\omega \omega/c$ and $k_{2\omega} = n_{2\omega} 2\omega/c$ are the wave vector amplitudes at the fundamental (ω) and SHG (2ω) frequencies, respectively [16]. With conventional nonlinear materials, this condition cannot be fulfilled, but it can be compensated by fabricating periodic quasi-phase-matched crystals [16,30,31]. It is also possible to utilize zero-index materials to realize structures that have relaxed phase-matching requirements [32].

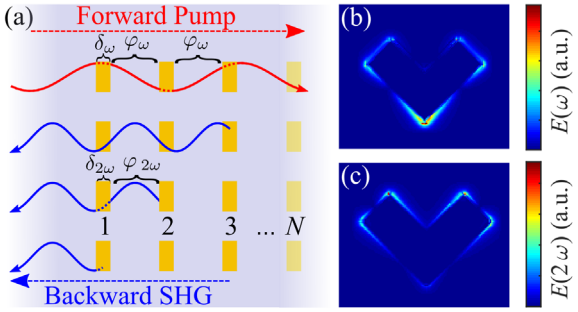

FIG. 2. (a) Backward phase-matched SHG emission from metamaterials consisting of N stacked layers. The phase-matching condition is fulfilled by controlling the phase accumulation for both incident light (red arrows) and SHG light (blue arrows). The terms φ_ω and $\varphi_{2\omega}$ correspond to phase accumulation due to propagation. The LSPRs of metal nanoantennas enhance the local fields at (b) fundamental frequency E_ω and (c) second-harmonic (SH) frequency $E_{2\omega}$ and also induce the phase changes associated with LSPRs δ_ω and $\delta_{2\omega}$, respectively.

By using resonant metamaterials, we can extend this phase-matching condition by taking into account the phase changes δ_ω and $\delta_{2\omega}$ that occur in a metamaterial due to coherent scattering of light from the constituent nanoantennas at the fundamental and SHG frequencies, respectively. Because these terms are dictated by the optical response of the nanoantennas, namely, by their LSPRs [7], the extended phase-matching condition becomes solvable by metamaterial design. In order to demonstrate this capability, we designed and fabricated metamaterial devices where the backward SHG emission is phase matched [see Fig. 2(a)].

The designed metamaterial devices consisted of a number N of identical metasurfaces that were separated by identical spacer layers of thickness h. For such devices, the total amplitude of the emitted SH field is described by (see the Supplemental Material [33] for details)

$$\mathrm{SHG} \propto \left| \sum_{J=1}^{N} T(\omega)^J T(2\omega)^{J/2} e^{iJ\Delta k} \chi^{(2)}_{\mathrm{ms}} E(\omega)^2 \right|^2, \quad (1)$$

where $\chi^{(2)}_{\mathrm{ms}}$ is the relevant component of the SHG susceptibility tensor of a single metasurface, and $T(\omega)$ and $T(2\omega)$ are the transmittances of a single metasurface at the fundamental and SH frequencies, respectively. For phase-matched SH emission, the wave vector mismatch Δk must therefore be an integer of 2π,

$$\Delta k = 2(\varphi_\omega + \delta_\omega) + \varphi_{2\omega} + \delta_{2\omega} = 2\pi m, \quad (2)$$

where m is an integer and terms $\varphi_{2\omega} = k_{2\omega} h$ and $\varphi_\omega = k_\omega h$ arise from the propagation of the fields. Estimating the

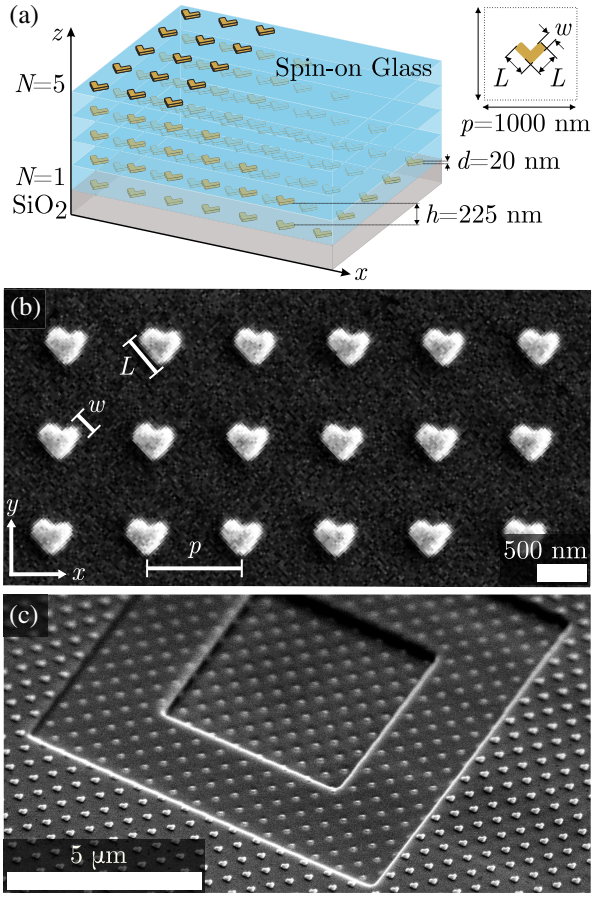

FIG. 3. (a) Investigated devices were composed of up to N metasurfaces stacked on top of each other, separated by $h = 225$-nm-thick spacer layers. Each of the metasurfaces consisted of a square array of 20-nm-thick V-shaped gold nanoantennas. (b) Representative scanning electron micrograph of one fabricated device ($L190$-3). (c) Oblique scanning electron micrograph obtained after successive etching with a focused ion beam, illustrating the stacked nature of the investigated metamaterial devices.

phase terms δ_ω and $\delta_{2\omega}$, which correspond to nanoparticles scattering phase retardation at ω and 2ω for the particles of interest, Eq. (2) allows us to solve for the spacer thickness h. The transmittance, phase, and susceptibility terms of Eqs. (1) and (2) were estimated from the measured transmission spectra of our devices (see the Supplemental Material [33] for details).

Our metamaterials consisted of a varying number N metasurfaces composed of V-shaped gold nanoantennas with arm lengths of $L = 190$ nm ($L190$-N), arm widths of $w = 100$ nm, and thicknesses of $d = 20$ nm. These nanostructures were arranged into square lattices with a lattice constant of $p = 1000$ nm [Fig. 3(a)]. This lattice configuration was chosen because it has been earlier found to emit SHG strongly [34]. However, we note that the configuration is not yet optimized in terms of overall conversion efficiency, because the strongest SHG emission from such arrays may not occur in the normal direction [35]. Note also that, due to the configuration, other nonlinear diffractive channels exist, but they do not fulfill the phase-matching condition. Interesting new possibilities to realize multibeam phase-matching processes can be envisioned in the context of multiplexed nonlinear metasurface stacks.

The above parameters were calculated to give rise to LSPRs centered near 1060 nm. According to Eq. (2), for $m = 0$ the phase-matching condition was fulfilled close to the LSPR wavelength by choosing the layer thickness of $h = 225$ nm. Specifically, the phase-matching condition for devices $L190$-N was fulfilled for linear input polarization orthogonal to the symmetry axis of the V particles (x axis) [Fig. 3(b)]. Because of the symmetry properties of the samples, the generated SHG emission is polarized along the symmetry axis (y axis).

The devices were fabricated using standard electron beam lithography on a cleaned SiO_2 substrate through a sequence of steps repeated N times (see the Supplemental Material [33] for further details) [36]. Representative scanning electron micrographs of one realized metamaterial device ($L190$-3) are shown in Figs. 3(b) and 3(c).

The SHG responses of the devices were characterized using a setup described in detail elsewhere [34]. Briefly, a femtosecond laser oscillator (Chameleon Vision II, Ti: sapphire, 80 MHz) combined with an optical parametric oscillator (Chameleon Compact, 1000–1300 nm) was used as the pump, while the backward-emitted SHG signals were measured using a power-calibrated photomultiplier tube. See Supplemental Material [33] for a more detailed description of the setup. Here, we limited our input mean power to 10 mW in order to avoid possible sample damage. The SHG responses of the fabricated metamaterial devices consisting of varying number of metasurfaces ($N = 1, 2, \ldots, 5$) were measured as a function of the pump wavelength (see Fig. 4).

The predicted SH emission spectra from the devices [Fig. 4(a)] show a clear increase of the average SHG power near the phase-matching wavelength of 1135 nm when the number of metasurfaces N grows. This behavior is also observed in the measured backward-emitted SHG signals [Fig. 4(b)]. The strongest SHG signal for the device composed of five metasurfaces ($L190$-5) corresponded to SHG power of 20 fW and occurred at the wavelength of 1141 nm, which is slightly shifted from the predicted phase-matching wavelength due to experimental imperfections. A closer analysis of the results reveals that the SHG response near 1141 nm no longer depends linearly on the number of metasurfaces N [Fig. 4(b)]. Instead, the SHG signals follow superlinear dependence on N ($\mathrm{SHG} \propto N^{1.27}$), confirming that the devices were successfully phase matched [Fig. 4(c)]. Furthermore, the devices were successfully phase matched in the challenging backward direction [37]. Because the SHG emission from the device $L190$-1 was markedly weaker than the SHG emissions

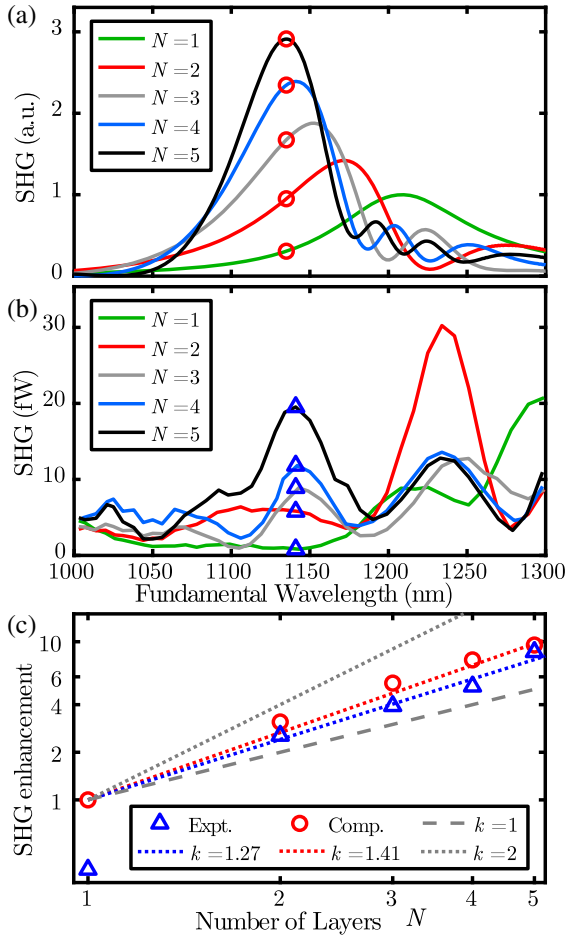

FIG. 4. (a) Predicted and (b) measured SHG emission spectra from the devices. SHG emission grows with increasing number of layers N at the phase-matching wavelength of 1135 nm (1141 nm) for predicted (measured) results. (c) Both the predicted (red spheres) and experimental (blue triangles) SHG emissions scale superlinearly as a function of N, resulting in linear fits with slopes $k > 1$ on the logarithmic scale.

from the rest of devices, that data point was excluded from the curve fitting. This difference between the $L190$-1 and other devices may be a result of interlayer coupling that is not present in the single layer device.

We note that the fabricated devices exhibited losses that were estimated by measuring the transmittance of a single metasurface to be close to 90% (97%) near the pump (SHG) wavelengths (see the measured transmittance spectra in the Supplemental Material [33]). By taking into account the associated reductions in the intensities for subsequent metasurfaces [see Eq. (1)], one expects around eightfold SHG enhancement, which is very close to the enhancement we measure [Fig. 4(c)].

Next we discuss approaches that could be combined with the demonstrated methodology in order to further improve the performance of nonlinear metamaterials. First, an obvious method would be to increase the number of metasurface stacks N. However, at some point of increasing N to values much higher than 5, the surface flatness of the fabricated metasurfaces may start to be affected. As discussed previously [38–40], the spin-on-glass planarization introduces surface roughness of the order of only a few nanometers for five adjacent layers. According to Ref. [41], some effort would be required to address this problem for thicker artificial nonlinear crystals (~20–50 layers and beyond). Second, the nanoparticle material, shapes, and dimensions used in this Letter have not yet been optimized in terms of overall conversion efficiencies. Recent advances in all-dielectric nonlinear metasurfaces also suggest that record-high conversion efficiencies could be achieved by phase matching such structures using this methodology [42]. Third, looking at Eq. (1) and Fig. 4(c), we see that, in order to considerably improve the efficiency of future phase-matched metamaterial devices by further increasing N, the metasurfaces should be made highly transparent at the operation wavelengths. Finally, we note that the conversion efficiency is not the only figure of merit. In many applications, a more important parameter is the optical power of the generated light. Here, nonlinear metasurfaces are a promising technology, because their fabrication can be scaled up to array sizes that are compatible with the use of high-power lasers, for example, by using nanoimprint lithography [43].

In addition to enhancing the overall conversion efficiencies of nonlinear metamaterials, this demonstration of phase-engineered nonlinear metamaterials has several other fundamental implications. For example, one can envisage how nonlinear metamaterials could be utilized for adiabatic frequency conversion, enabling broadband frequency conversion in nanomaterials [44,45]. Furthermore, this methodology could allow design of more efficient nonlinear terahertz-emitting metamaterials [46–48]. Finally, the presented phase-engineering principles apply also for arbitrary wave fronts. Successful phase matching of nonlinear processes using complex spatial modes would have applications in holography and quantum computing [24,28].

To conclude, we have demonstrated how the performance of nonlinear metamaterials can be substantially increased by stacking metasurfaces into three-dimensional metamaterials. Phase-matching considerations that are often difficult to fulfill using conventional materials can be easily solved by controlling the dimensions of the nanoantennas and the separation between the metasurfaces. We demonstrated this by phase matching second-harmonic generation emission from fabricated metamaterials in the challenging backward direction. We fabricated nonlinear metamaterial devices consisting of up to five stacked metasurfaces and demonstrated an order-of-magnitude increase in the backward-emitted second-harmonic intensities from the devices. Our results open a new paradigm of phase-engineered three-dimensional nonlinear metamaterials that could be used, for example, to realize more efficient nonlinear metamaterials.

We acknowledge the support of the Academy of Finland (Grant No. 308596), the Flagship of Photonics Research and Innovation (PREIN) funded by the Academy of Finland (Grant No. 320165), the European Research Council (ERC) under the European Union's Horizon 2020 Research and Innovation Programme (Grant Agreements No. 639109 and No. 724881), the National Research Foundation (NRF) Grants (No. NRF-2019R1A2C3003129, No. CAMM-2019M3A6B3030637, No. NRF-2019R1A5A8080290, and No. NRF-2020K1A3A1A21024374) funded by the Ministry of Science and ICT of the Korean Government. Younghwan Yang acknowledges a fellowship from Hyundai Motor Chung Mong-Koo Foundation, and Minkyung Kim acknowledges the NRF Global Ph.D. fellowship (NRF-2017H1A2A1043204) funded by the Ministry of Education of the Korean government.

*These authors contributed equally to this work.
†Corresponding author.
patrice.genevet@crhea.cnrs.fr
‡Corresponding author.
jsrho@postech.ac.kr

[1] C. M. Soukoulis and M. Wegener, Nat. Photonics **5**, 523 (2011).
[2] M. W. Klein, C. Enkrich, M. Wegener, and S. Linden, Science **313**, 502 (2006).
[3] A. Alù, M. G. Silveirinha, A. Salandrino, and N. Engheta, Phys. Rev. B **75**, 155410 (2007).
[4] S. Zhang, Y.-S. Park, J. Li, X. Lu, W. Zhang, and X. Zhang, Phys. Rev. Lett. **102**, 023901 (2009).
[5] N. Yu and F. Capasso, Nat. Mater. **13**, 139 (2014).
[6] X. Yin, T. Steinle, L. Huang, T. Taubner, M. Wuttig, T. Zentgraf, and H. Giessen, Light **6**, e17016 (2017).
[7] P. Genevet, F. Capasso, F. Aieta, M. Khorasaninejad, and R. Devlin, Optica **4**, 139 (2017).
[8] L. Huang, S. Zhang, and T. Zentgraf, Nanophotonics **7**, 1169 (2018).
[9] E. Arbabi, S. M. Kamali, A. Arbabi, and A. Faraon, ACS Photonics **5**, 3132 (2018).
[10] H. Ren, G. Briere, X. Fang, P. Ni, R. Sawant, S. Héron, S. Chenot, S. Vézian, B. Damilano, V. Brändli, S. A. Maier, and P. Genevet, Nat. Commun. **10**, 2986 (2019).
[11] N. A. Rubin, G. D'Aversa, P. Chevalier, Z. Shi, W. T. Chen, and F. Capasso, Science **365**, eaax1839 (2019).
[12] P. G. Kwiat, K. Mattle, H. Weinfurter, A. Zeilinger, A. V. Sergienko, and Y. Shih, Phys. Rev. Lett. **75**, 4337 (1995).
[13] T. Brabec and F. Krausz, Rev. Mod. Phys. **72**, 545 (2000).
[14] T. J. Kippenberg, R. Holzwarth, and S. A. Diddams, Science **332**, 555 (2011).
[15] M. R. Shcherbakov, P. P. Vabishchevich, A. S. Shorokhov, K. E. Chong, D. Y. Choi, I. Staude, A. E. Miroshnichenko, D. N. Neshev, A. A. Fedyanin, and Y. S. Kivshar, Nano Lett. **15**, 6985 (2015).
[16] R. W. Boyd, *Nonlinear Optics* (Academic Press, San Diego, 2020).
[17] C. Wang, Z. Li, M. H. Kim, X. Xiong, X. F. Ren, G. C. Guo, N. Yu, and M. Lončar, Nat. Commun. **8**, 2098 (2017).
[18] E. J. Lim, M. M. Fejer, and R. L. Byer, Electron. Lett. **25**, 174 (1989).
[19] M. Kauranen and A. V. Zayats, Nat. Photonics **6**, 737 (2012).
[20] J. Lee, M. Tymchenko, C. Argyropoulos, P. Y. Chen, F. Lu, F. Demmerle, G. Boehm, M. C. Amann, A. Alù, and M. A. Belkin, Nature (London) **511**, 65 (2014).
[21] S. A. Maier, *Plasmonics: Fundamentals and Applications* (Springer Science & Business Media, New York, 2007).
[22] M. Lapine, I. V. Shadrivov, and Y. S. Kivshar, Rev. Mod. Phys. **86**, 1093 (2014).
[23] J. Butet, P. F. Brevet, and O. J. Martin, ACS Nano **9**, 10545 (2015).
[24] G. Li, S. Zhang, and T. Zentgraf, Nat. Rev. Mater. **2**, 17010 (2017).
[25] E. Rahimi and R. Gordon, Adv. Opt. Mater. **6**, 1800274 (2018).
[26] M. J. Huttunen, R. Czaplicki, and M. Kauranen, J. Nonlinear Opt. Phys. Mater. **28**, 1950001 (2019).
[27] N. Segal, S. Keren-Zur, N. Hendler, and T. Ellenbogen, Nat. Photonics **9**, 180 (2015).
[28] G. Li, S. Chen, N. Pholchai, B. Reineke, P. W. H. Wong, E. Y. B. Pun, K. W. Cheah, T. Zentgraf, and S. Zhang, Nat. Mater. **14**, 607 (2015).
[29] C. Schlickriede, N. Waterman, B. Reineke, P. Georgi, G. Li, S. Zhang, and T. Zentgraf, Adv. Mater. **30**, 1703843 (2018).
[30] M. Pelton, P. Marsden, D. Ljunggren, M. Tengner, A. Karlsson, A. Fragemann, C. Canalias, and F. Laurell, Opt. Express **12**, 3573 (2004).
[31] X. P. Hu, P. Xu, and S. N. Zhu, Photonics Res. **1**, 171 (2013).
[32] H. Suchowski, K. O'Brien, Z. J. Wong, A. Salandrino, X. Yin, and X. Zhang, Science **342**, 1223 (2013).
[33] See Supplemental Material at http://link.aps.org/supplemental/10.1103/PhysRevLett.126.033901 for descriptions of the semi-analytical phase-matching model, the sample fabrication process, the transmission experiments, and the experimental setup.
[34] R. Czaplicki, A. Kiviniemi, M. J. Huttunen, X. Zang, T. Stolt, I. Vartiainen, J. Butet, M. Kuittinen, O. J. F. Martin, and M. Kauranen, Nano Lett. **18**, 7709 (2018).
[35] R. Czaplicki, A. Kiviniemi, J. Laukkanen, J. Lehtolahti, M. Kuittinen, and M. Kauranen, Opt. Lett. **41**, 2684 (2016).
[36] G. Yoon, I. Kim, S. So, J. Mun, M. Kim, and J. Rho, Sci. Rep. **7**, 6668 (2017).
[37] L. Liu, L. Wu, J. Zhang, Z. Li, B. Zhang, and Y. Luo, Adv. Sci. **5**, 1800661 (2018).
[38] A. Arbabi, E. Arbabi, S. M. Kamali, Y. Horie, S. Han, and A. Faraon, Nat. Commun. **7**, 13682 (2016).
[39] L. Yan, W. Zhu, M. F. Karim, H. Cai, A. Y. Gu, Z. Shen, P. H. J. Chong, D. L. Kwong, C. W. Qiu, and A. Q. Liu, Adv. Mater. **30**, 1802721 (2018).
[40] C. Jin, M. Afsharnia, R. Berlich, S. Fasold, C. Zou, D. Arslan, I. Staude, T. Pertsch, and F. Setzpfandt, Adv. Photonics **1**, 1 (2019).
[41] Y. Zhao, M. A. Belkin, and A. Alù, Nat. Commun. **3**, 870 (2012).
[42] B. Sain, C. Meier, and T. Zentgraf, Adv. Photonics **1**, 1 (2019).
[43] J. M. Kontio, H. Husu, J. Simonen, M. J. Huttunen, J. Tommila, M. Pessa, and M. Kauranen, Opt. Lett. **34**, 1979 (2009).

[44] H. Suchowski, D. Oron, A. Arie, and Y. Silberberg, Phys. Rev. A **78**, 063821 (2008).
[45] H. Suchowski, V. Prabhudesai, D. Oron, A. Arie, and Y. Silberberg, Opt. Express **17**, 12731 (2009).
[46] D. K. Polyushkin, E. Hendry, E. K. Stone, and W. L. Barnes, Nano Lett. **11**, 4718 (2011).
[47] L. Luo, I. Chatzakis, J. Wang, F. B. Niesler, M. Wegener, T. Koschny, and C. M. Soukoulis, Nat. Commun. **5**, 3055 (2014).
[48] S. Keren-Zur, M. Tal, S. Fleischer, D. M. Mittleman, and T. Ellenbogen, Nat. Commun. **10**, 1778 (2019).